Polymer Degradation and Stability 98 (2013) 2153–2160

Contents lists available at ScienceDirect

Polymer Degradation and Stability

journal homepage: www.elsevier.com/locate/polydegstab

Flame retardant high density polyethylene optimized by on-line ultrasound extrusion

G. Sanchez-Olivares [a, *], A. Sanchez-Solis [b], F. Calderas [b], L. Medina-Torres [c], E.E. Herrera-Valencia [c], J.I. Castro-Aranda [a], O. Manero [b], A. Di Blasio [d], J. Alongi [d]

[a] CIATEC, A.C., Omega 201, León, Gto. 37545, Mexico
[b] Instituto de Investigaciones en Materiales, Universidad Nacional Autónoma de México, Apartado Postal 70-360, México D.F. 04510, Mexico
[c] Facultad de Química, Universidad Nacional Autónoma de México, Ciudad Universitaria, México D.F. 04510, Mexico
[d] Politecnico Di Torino, Viale Teresa Michel 5, Alessandria 15121, Italy

ARTICLE INFO

Article history:
Received 22 July 2013
Accepted 4 September 2013
Available online 14 September 2013

Keywords:
HDPE
Flame retardant properties
Ultrasound extrusion
ATH

ABSTRACT

The effect of on-line ultrasound application by a special static mixer die which promotes extensional flow simultaneously during the single screw extrusion process was thoroughly studied. The proportion of aluminum trihydroxide (ATH) used as flame retardant on high density polyethylene (HDPE) was optimized. The morphological, thermal, flammability, combustion, mechanical and rheological properties of the materials were investigated. The morphological study pointed out that this process is able to strongly reduce the size of ATH particles and improve their dispersion and distribution within the polymer matrix. The addition of zinc borate (ZB) at low concentration (namely 3 phr) showed its well-known synergistic effect in the thermal, oxygen index and fire combustion behavior. According to the UL94 standard, the rating for all materials tested changed from HB to V2, with respect to materials prepared without ultrasound; furthermore a rating V0 was achieved only with the addition of 2 phr organo-clay. Rheological results under simple and small amplitude oscillatory shear flow confirmed the enhanced particle dispersion and finer particle morphology evidenced by larger values of the moduli and by deviations from the semicircular shape observed in the Cole–Cole diagram. Mechanical properties such as Izod impact resistance, tensile strength, strain at break and tenacity were also improved by the on-line ultrasound process. In this work, the appropriate on-line ultrasound extrusion conditions to use the lowest ATH content (30 phr or 21.5 in wt%) were found, rendering HDPE optimized flame retardant materials with improved processability and mechanical properties.

1. Introduction

Additives for flame retardant polymers include metal hydroxides, which are some of the most used non-halogen flame retardant additives due to their low cost and toxicity, easy of handling and minimal corrosion effects. Furthermore, during polymer combustion they can also reduce smoke emission. In particular, aluminum trihydroxide (ATH) is the most commonly used metal hydroxide, specially in elastomers, thermoplastic, and thermosetting resins [1]. The main disadvantage in the use of ATH is the large content (40-65 wt%) necessary to produce flame retardant polymers suitable for demanding applications, V0 classification according to UL94 standards. This high load has negative effects on the mechanical properties of the polymer matrix [2]. On the other hand, it is well known that zinc borate (ZB) has an important synergistic effect in combination with ATH, resulting in an important reduction on ATH content [3]. Bourbigot et al. [4] thoroughly investigated the synergistic effect of ZB and ATH on EVA. The authors proposed that ATH decomposes by an endothermic reaction in Al_2O_3 as a first event, and then the polymer forms a cross-linked network and a carbonaceous char, which limits the degradation of the polymer. At the same time, ZB forms a vitreous phase providing a more effective char. The authors reported a significant increase in thermal stability in air, oxygen index and ignition time as well as an important reduction on EVA combustion rate, substituting partially ATH with ZB (total content 65%). Hull et al. [5] investigated the combustion

* Corresponding author. Tel./fax: +52 4777100011.
E-mail addresses: sanchezolivaresg@gmail.com, gsanchez@ciatec.mx (G. Sanchez-Olivares), sancheza@unam.mx (A. Sanchez-Solis), faustocg@unam.mx (F. Calderas), luismt@unam.mx (L. Medina-Torres), edtson_ed@hotmail.com (E.E. Herrera-Valencia), isbell_ca@hotmail.com (J.I. Castro-Aranda), manero@unam.mx (O. Manero), alessandro.diblasio@polito.it (A. Di Blasio), jenny.alongi@polito.it (J. Alongi).

0141-3910/$ – see front matter © 2013 Elsevier Ltd. All rights reserved.
http://dx.doi.org/10.1016/j.polymdegradstab.2013.09.001

toxicity of EVA using ATH/ZB additives at 70% as total amount; this system presented a significant reduction of CO yield with respect to the pure copolymer. The authors attributed the result to the effectiveness of the fillers which reduce the oxidation of the residual organic material under fuel rich conditions.

In another context, on-line ultrasound extrusion is a processing method that has been reported to enhance particles dispersion at nanometric level [6,7]. Swain and Isayev [8] studied the effect of continuous ultrasonic treatment during the melt intercalation of HDPE into montmorillonite clay on their structural, mechanical, rheological and oxygen barrier properties. The authors evaluated the effect of the clay at different content (namely, 2.5, 5.0 and 10.0 wt%); the nanocomposites were prepared using a single screw extruder attached with an ultrasonic slit die, operating at a frequency of 20 KHz and amplitudes of 5, 7.5 and 10 μm. High dispersion of clay in the HDPE matrix and higher complex viscosity due to the ultrasonic treatment were reported. Mechanical properties were improved and oxygen permeability was substantially decreased after ultrasonic treatment.

In this work, the effect of the on-line ultrasound application during the extrusion process of HDPE with flame-retardant additives (ATH, ZB and OBEN) is studied in detail. The ultrasonic transducers are attached to a special mixer die. This experimental arrangement is intended to improve additive particle dispersion and distribution in the HDPE matrix. It is expected that the processing of these materials would be largely improved and hence the flame retardant properties, avoiding the use of high additive loads that have a negative effect on the mechanical properties of the compounds.

2. Experimental part

2.1. Materials

High density polyethylene (referred from here on as PE) from PEMEX, México, sodium bentonite clay (BEN) Actisil 220FF, with 55 meq/100 g ionic interchange capacity from Süd-Chemie, L-lysine mono-chlorohydrated aminoacid (Lys), industrial grade aluminum trihydroxide ($Al(OH)_3$) with 99.5% purity and surface area of 12 m^2/g, zinc borate ($2ZnO.3B_2O_3.3.5H_2O$), maleic anhydride (MAH) and benzoyl peroxide (BOP) were used as received.

2.2. Equipment

The PE, flame retardant additives and clay were processed in a twin screw counter-rotating extruder, Leistritz Micro 27 with L/D = 32 and diameter of 27 mm; alternatively, a single screw extruder with L/D = 24 and diameter of 25.4 mm was coupled to a static mixer die which promotes extensional flow assisted by ultrasonic elements to generate ultrasonic waves. Details of this device and application conditions of ultrasonic waves have been reported elsewhere [9]. Injection molding process was carried out in a Milacron M50 injection molding machine.

2.3. Procedure

Preparation of materials included the bentonite clay modification via ionic interchange reaction using L-lysine amino-acid as intercalate agent to produce organoclay (OBEN) [10–12]. In order to improve PE and OBEN affinity, a compatibilizer based on PE and MHA ($PE_{-g\text{-}MAH}$) was produced by reactive extrusion. The grafting reaction was carried out in a twin screw extruder at 195 °C (mixer zone) and 50 rpm screw speed using BOP as initiator [13].

Table 1
Materials composition based on PE.

Sample code	Extrusion process	ATH [phr]	ZB [phr]	OBEN [phr]	$PE_{-g\text{-}MAH}$ [phr]
PE	–	–	–	–	–
PE-ATH_{50}	TS	50	0	0	0
PE-ATH_{30}/ZB_5	TS	30	5	0	0
PE-ATH_{30}/ZB_5/US	SS-US	30	5	0	0
PE-ATH_{30}/ZB_3	TS	30	3	0	0
PE-ATH_{30}/ZB_3/US	SS-US	30	3	0	0
PE-$ATH_{30}/ZB_3/OBEN_1$	TS	30	3	1	2
PE-$ATH_{30}/ZB_3/OBEN_1$/US	SS-US	30	3	1	2
PE-$ATH_{30}/ZB_3/OBEN_2$	TS	30	3	2	4
PE-$ATH_{30}/ZB_3/OBEN_2$/US	SS-US	30	3	2	4

2.4. Processing

1. Twin screw extrusion (TS): materials were compounding according to Table 1, using the twin-screw extruder. The temperature at the mixer zone was set to 195 °C and the rotation speed at 200 rpm.
2. Single screw-ultrasound assisted extrusion (SS-US): materials extruded by on-line ultrasound were compounding according to stage 1, afterwards they were extruded in the single screw extruder/static mixer die assisted with the ultrasound system. The temperature at mixer zone and the rotation speed were set to 200 °C and 30 rpm, respectively.
3. Suitable samples for UL94, LOI, cone calorimetric and mechanical tests of the materials compounding in stages 1–2, were obtained by injection molding at a temperature of 210 °C and injection speed of 70 mm/s.

2.5. Characterization

Flame retardant properties were evaluated by the UL94 classification, according to ASTM D635 (IEC60695-11) in horizontal position and ASTM D3801 (IEC 707-9 e ISO 1210) in vertical position. Sample dimensions were 125 × 13 × 3 mm, maintained at 23 °C and 50% humidity during 48 h prior to analysis. Limiting Oxygen Index (LOI) tests were performed with a FIRE oxygen index apparatus according to ISO 4589. The combustion behavior was studied by cone calorimetric (Fire Testing Technology, FTT) according to the ISO 5660 standard. The measurements were carried out under a 35 kW/m^2 irradiative heat flux, in horizontal configuration, sample dimensions: 100 × 100 × 3 mm. All measurements were performed in triplicate in order to have reproducible data and the results were averaged. Thermogravimetric analysis (TGA) was carried out in a TA-Instruments Q500 calorimeter with heating rate of 10 °C/min under argon atmosphere. Micrographs were taken in a field-emission scanning electron microscope (SEM) Jeol JSM-7600F. Rheological measurements were carried out in a stress-controlled TA-G2 rheometer using the parallel-plates fixture with 25 mm diameter and a heating chamber (TA-Extended Temperature System). The rheological tests were performed at 190 °C, using 0.75 mm gap, particularly, the oscillatory tests were carried out in the linear viscoelastic regime, i.e. under small amplitude oscillatory shear (SAOS) flow.

3. Results and discussion

3.1. Morphology

The morphology of the investigated materials was studied by Scanning Electron Microscopy (SEM). Fig. 1 shows SEM micrograph of the fractured surface of the neat polymer matrix and some investigated materials (namely: (a) PE, (b) PE-ATH_{50}, (c) PE-ATH_{30}/

ZnB_3, (d) PE-ATH_{30}/ZnB_3/US, (e) PE-ATH_{30}/ZnB_3/$OBEN_2$ and (f) PE-ATH_{30}/ZnB_3/$OBEN_2$/US). According to Fig. 1, the morphology of PE (Fig. 1a) shows a ductile fracture typically observed in a high density polyethylene. For the materials produced by TS (Fig. 1b,c,e), many agglomerates of the ATH particles are observed, in materials with both high and low ATH content (50 and 30 phr, respectively), with size around 1-3 microns depicting poor adhesion with the polymer matrix. The low adhesion of ATH particles is observed by the empty holes and interstices between particles and polymer matrix, illustrating the problem to achieve an adequate level of dispersion and distribution of the additives when large ATH concentrations are employed, even though a high screw speed was used (200 rpm). The morphology of the materials obtained by SS-US is depicted in Fig. 1d and f; the micrographs show an important effect of the on-line ultrasound system on the dispersion and distribution of ATH particles. The PE-ATH_{30}/ZnB_3/US material (Fig. 1d), shows smaller ATH particles size (around 1 micron or less) than that of the materials obtained by TS (Fig. 1c), demonstrating the on-line ultrasound effect on morphology. On the other hand, this effect is notably more evident in the PE-ATH_{30}/ZnB_3/$OBEN_2$/US morphology (Fig. 1f), since no agglomerates of ATH particles are present; in fact no particles are observed on the fractured surface. This morphology is attributed to ATH particles size being greatly reduced, probably smaller than 1 micron. This effect is presumably caused by both ultrasound and improved ATH-matrix-OBEN affinity, due to the $PE_{\text{-g-MAH}}$ compatibilizer action [14,15]. To confirm the dispersion and distribution level of ATH additive, Fig. 2 shows elemental analysis carried out by energy dispersive spectroscopy (EDS) of the PE-ATH_{30}/ZB_3/$OBEN_2$/US material. Fig. 2a and b depict the SEM magnification and aluminum elemental analysis, respectively; a good dispersion and a fine distribution of the aluminum element in PE matrix are observed. According to the morphological study (Figs. 1 and 2), the on-line ultrasound application improved the dispersion and distribution and reduced the size of the ATH particles considerably. Zinc borate particles were not observed in micrographs, probably due to their low content (3 phr) and/or because of their very good dispersion and distribution in the matrix. Clay particles were dispersed possibly up to nanometric scale.

3.2. Thermal stability

Thermal stability of ATH and ZB additives employed in this work was evaluated by TGA under argon atmosphere. Fig. 3 depicts the thermogravimetric curves and Table 2 disclosed the data. Specifically T_{onset} corresponding to the temperature at which 2% of weight loss has occurred and T_{max} was obtained from the derivative

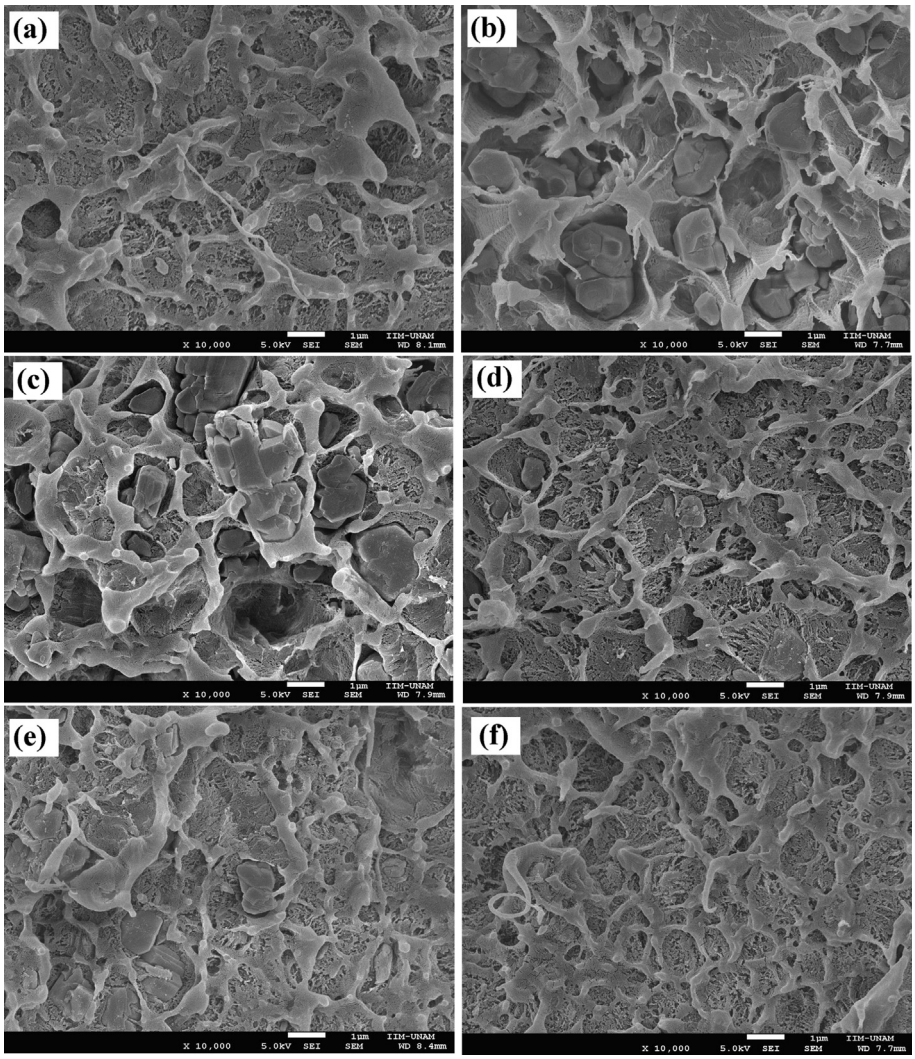

Fig. 1. SEM micrographs of fractured surface. (a) PE, (b) PE-ATH_{50}, (c) PE-ATH_{30}/ZnB_3, (d) PE-ATH_{30}/ZnB_3/US, (e) PE-ATH_{30}/ZnB_3/$OBEN_2$ and (f) PE-ATH_{30}/ZnB_3/$OBEN_2$/US 10,000× magnification.

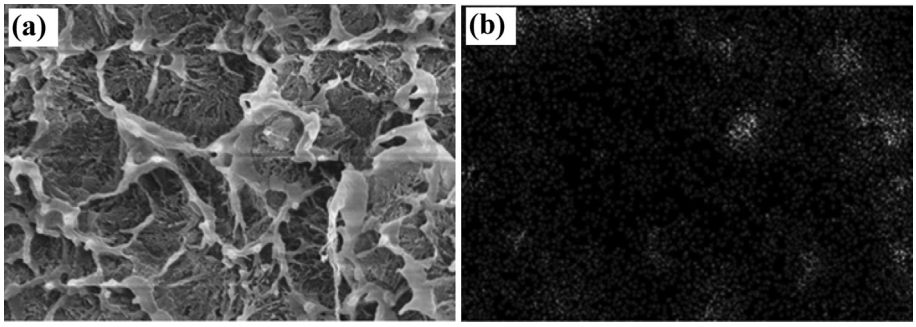

Fig. 2. EDS analysis of the PE-$ATH_{30}/ZB_3/OBEN_2$/US material. a) SEM image and b) Aluminum elemental analysis.

signal (dTG). As it is well known, ATH is a flame retardant additive with lower thermal stability than ZB. ATH thermal decomposition started at 222 °C (T_{oneset}) and its main decomposition is reached at 230 °C (T_{max}). At this point almost 30 wt% is lost due to the start of the decomposition reaction [$2Al(OH)_3 \rightarrow Al_2O_3 + 3H_2O$]; afterwards ATH decomposes slowly up to a stabilization at nearly 600 °C, where 67 wt% total residues were produced. However ZB exhibited the usual thermal stability; T_{onset} was reached at 308 °C and the main decomposition temperature was recorded at 385 °C. Within this temperature range ZB decomposes releasing crystallization water molecules, and the main weight loss (12%) occurred at 396 °C. ZB reaches stability faster than ATH and presented 20% more residues production (87 wt%).

Fig. 4 shows the thermogravimetric curves of the neat polymer matrix and all investigated materials. The results are summarized in Table 3. Onset temperatures 1 and 2 were defined as the value at which 2 and 12% weight loss occurred, respectively. T_{max} was obtained from dTG curve corresponding to the maximum decomposition temperature. According to Fig. 4 and Table 3, for all investigated materials, T_{onset1} started at lower temperature than that of pure PE (348 °C). The materials showed a T_{onset1} within the same range (248–261 °C), which indicated that all additives ATH, ZB, OBEN and the extrusion processes did not promote the anticipation of PE decomposition process, attributed to low thermal stability of ATH, as discussed before. Nevertheless, T_{onset2} and T_{max} are clearly increased. $T_{oneset2}$ increased from 355 to 372 °C, for PE-ATH_{50} and PE-ATH_{30}/ZB_3. The highest values of $T_{oneset2}$ were observed in PE-ATH_{30}/ZB_5, PE-ATH_{30}/ZB_3/US and PE-$ATH_{30}/ZB_3/OBEN_1$/US materials with 396, 396 and 397 °C respectively. The main enhancement was observed in T_{max}, increasing from 372 °C (PE) to 420 °C for PE-$ATH_{30}/ZB_3/OBEN_1$ and PE-$ATH_{30}/ZB_3/OBEN_1$/US materials, these results demonstrated that the addition of ATH/ZB and OBEN increased the main decomposition temperature of PE in both extrusion processes. A synergistic effect due to the combination of ATH/ZB was observed on thermal stability reducing the overall concentration level. Residues at 600 °C indicated char-forming capacity of the additives.

3.3. Flame retardant properties

Table 4 presents flame retardant properties according to UL94 classification of the materials produced by both extrusion processes, TS and SS-US. Results showed that the material produced with high ATH content (PE-ATH_{50}) using TS renders an optimum V0 classification. This result is not surprising considering that, at high concentrations, the flame retardant additives are very effective; however when ATH content is diminished to 30 phr, no UL94-V classification is reached, even though ZB was added at different contents (5 and 3 phr). According to the current literature, it is well known that the combination of zinc borate with metal hydroxide additives gives a synergistic effect in the flame retardant properties of polymers [3]; in our case, when the materials are processed by TS, this synergistic effect is not observed in PE-ATH system; the burning rates of PE-ATH_{30}/ZB_5 and PE-ATH_{30}/ZB_3 (21.9 and 23.6 mm/min) materials are quite similar to PE (25.2 mm/min). The presence of OBEN (1 and 2 phr) in the PE-ATH_{30}/ZB_3 showed a slight reduction on burning rate, nevertheless this result is not an important reduction in flammability. However, when the same materials are processed by SS-US, most of them are classified as V2 and one as V0 (PE-$ATH_{30}/ZB_3/OBEN_2$/US). These results clearly showed the effect of the on-line ultrasound and the OBEN presence, which improves flame retardant properties due to good dispersion and distribution of additive particles (ATH, ZB and OBEN) in the polymer matrix. In the case of PE-$ATH_{30}/ZB_3/OBEN_2$/US material, which was the only one with V0 classification, this result is attributed to a good affinity between OBEN particles and polymer matrix due to $PE_{-g\text{-}MAH}$ addition, which also contributes to a good dispersion of the particles (probably up to nanometric scale). The OBEN content is therefore important to achieve good flame retardant properties, because with only a 2 phr content a V0 classification is obtained. With a lower content (1 phr) particles and flame retardant additives are unable to produce an efficient char layer as a physical barrier during the combustion process. According to UL94-V results, the materials processed by SS-US could have an important commercial exploitation due to reduction in additive content and cost.

To summarize the main mechanisms proposed for the ATH and ZB additives action on the flame retardant properties, the following steps are considered: A) ATH decomposes through an endothermic reaction, which absorbs heat. B) ATH releases water vapor from

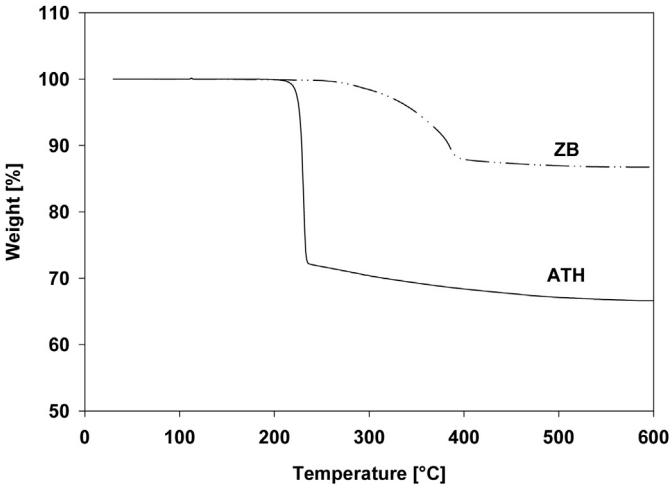

Fig. 3. Thermogravimetric curves of ATH and ZB additives.

Table 2
Thermogravimetric results of ATH and ZB.

Sample	T_{onset} [°C]	T_{max} [°C]	Residue at 600 °C [wt %]
ATH	222	230	67
ZB	308	385	87

hydroxyl group bonded with aluminum. The water released dilutes flammable gases during combustion process. C) ATH has a higher heat capacity than most polymers, which contributes to promote the "cooling effect" of the polymer matrix. D) ATH forms a protective layer of Al_2O_3 due to ATH decomposition. E) ZB acts as a flame retardant in both condensed and gas phases; at high temperature ZB releases crystallization water which contributes to the dilution of flammable gases. After its decomposition, ZB forms a vitreous layer at the polymer surface [16].

3.4. Limiting oxygen index

In order to evaluate in detail the effect of ultrasound application and the influence of OBEN particles on flame retardant properties under controlled atmosphere and combustion behavior, PE, PE-ATH_{50}, PE-ATH_{30}/ZB_3, PE-ATH_{30}/ZB_3/US, PE-$ATH_{30}/ZB_3/OBEN_2$, PE-$ATH_{30}/ZB_3/OBEN_2$/US materials were selected to be characterized by oxygen index and cone calorimetric tests.

Table 5 discloses the minimum oxygen percentage required to maintain flame under combustion (LOI, %) of the selected materials. PE-ATH_{50} presented the highest value (22.1%) with respect to PE (19.7%), probably due to dilution of combustible products with a high ATH content; however, this result was not significant. Oxygen index percentage of PE-ATH_{30}/ZB_3 and PE-$ATH_{30}/ZB_3/OBEN_2$ materials processed by TS and SS-US is almost the same (21.5–21.9%). Values were slightly higher than PE (19.7%), revealing no significant improvement in flammability. LOI results showed that the ATH and its combination with ZB in PE matrix do not have an important gas phase activity as flame inhibitors. It is important to observe that according to these results, on-line ultrasound application (dispersion and distribution of additive particles) did not influence the flammability of the materials under controlled atmosphere.

3.5. Combustion behavior

Table 6 discloses cone calorimetric data; Time To Ignition (TTI), the maximum Heat Release Rate (HRR) peak (pkHRR), Total Heat Evolved (THE), Total Smoke Release (TSR), CO and CO_2 yield and residue formed for PE, PE-ATH_{50}, PE-ATH_{30}/ZB_3, PE-ATH_{30}/ZB_3/US, PE-$ATH_{30}/ZB_3/OBEN_2$ and PE-$ATH_{30}/ZB_3/OBEN_2$/US materials. Results clearly showed the additives effect on combustion behavior, since pkHRR decreased considerably for all investigated materials with respect to PE. The largest reduction (−46%) was observed in the PE-ATH_{50} material, probably due to the highest ATH content; however materials PE-$ATH_{30}/ZB_3/OBEN_2$/US presented similar reductions (−43%) in spite of the low ATH content, which confirms the synergistic effect of the ZB in combination with ATH. With respect to THE, the value remained close to 119–123 MJ/m^2 for all materials. These results revealed no significant changes in total heat release at the end of the test. Schartel et al. [17] has pointed out that the reduction in HRR without any change in THE indicates a physical barrier without decreasing the total amount of combustible material. Accordingly, ATH, ATH/BZ and ATH/BZ/OBEN combinations presented similar barrier effect, independently of the extrusion process. TSR increased similarly in all materials; this increase is attributed to the release of non-flammable products (H_2O, CO_2) of ATH due to an endothermic mechanism. According to CO_2 yield in Table 2, the results confirm this mechanism. The residue production depends on additive content, attributed to the char layer mechanism for ATH, ZB and OBEN.

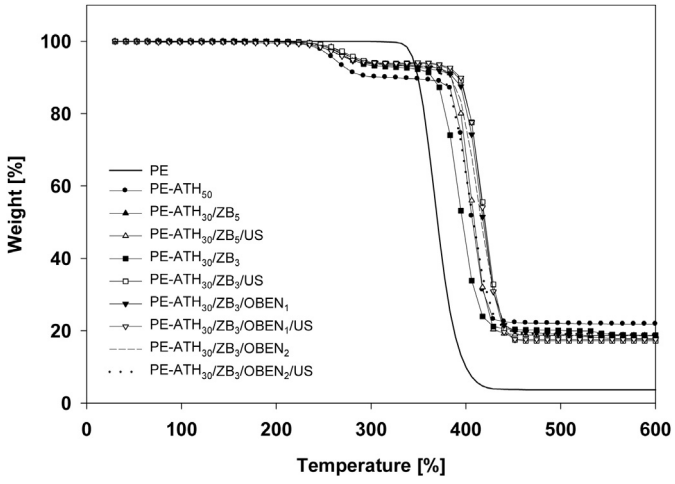

Fig. 4. Thermogravimetric curves of PE and investigated materials.

Table 3
Thermogravimetric results of PE and investigated materials.

Sample	T_{onset1} [°C]	$T_{oneset2}$ [°C]	T_{max} [°C]	Residue at 600 °C [wt %]
PE	348	355	372	3.8
PE-ATH_{50}	248	372	403	21.8
PE-ATH_{30}/ZB_5	255	396	406	19.0
PE-ATH_{30}/ZB_5/US	261	391	408	18.7
PE-ATH_{30}/ZB_3	254	372	396	18.7
PE-ATH_{30}/ZB_3/US	257	396	418	17.2
PE-$ATH_{30}/ZB_3/OBEN_1$	252	391	420	17.8
PE-$ATH_{30}/ZB_3/OBEN_1$/US	247	397	420	17.5
PE-$ATH_{30}/ZB_3/OBEN_2$	250	391	417	18.5
PE-$ATH_{30}/ZB_3/OBEN_2$/US	248	381	412	19.0

The heat release rate (HRR) curves obtained under forced flaming combustion for the investigated materials are depicted in Figs. 5 and 6. According to Fig. 5, high density polyethylene presented a typical pattern of a high flammable polymer, meanwhile, the materials containing flame retardant additives and OBEN showed a notable decrease in HRR. The reduction of HRR is accompanied by a pronounced prolongation of burning time, indicating an important barrier mechanism at the surface [18] that hindered the mass or heat transport between the flame zone and condensed phase. This barrier mechanism was presented in all investigated materials, confirming the effectiveness of ATH at high content (50 phr) and the synergistic effect of ZB and ATH in combustion behavior. This behavior was independent of OBEN addition and the extrusion process. However, depending on the extrusion

Table 4
UL94 classification results, vertical (rating) and horizontal (burning rate, mm/min) position.

Sample	Flammability results	
	Twin screw	Single screw/ultrasound
PE	25.2	–
PE-ATH_{50}	V0	–
PE-ATH_{30}/ZB_5	21.9	V2
PE-ATH_{30}/ZB_3	23.6	V2
PE-$ATH_{30}/ZB_3/OBEN_1$	20.2	V2
PE-$ATH_{30}/ZB_3/OBEN_2$	19.0	V0

Table 5
Limiting oxygen index results of selected materials.

Sample	LOI [%]
PE	19.7
PE-ATH$_{50}$	22.1
PE-ATH$_{30}$/ZB$_3$	21.7
PE-ATH$_{30}$/ZB$_3$/US	21.5
PE-ATH$_{30}$/ZB$_3$/OBEN$_2$	21.9
PE-ATH$_{30}$/ZB$_3$/OBEN$_2$/US	21.9

process, a different HRR pattern is presented. Fig. 5 shows that materials obtained by TS presented a typical "thick charring" pattern, which is characterized by a substantial increase of HRR at the start of the combustion until the char layer is formed, followed by a remarkable HRR decrease [19]. The HRR pattern was clearly modified by the ultrasound application (Fig. 6). At the start of combustion process these materials show an increase of HRR, but it is not as large as the thick charring pattern. Char layer is probably built up slowly to reach a maximum HRR, therefore at this point pkHRR is delayed and diminished. Probably, the OBEN, ZB and small amounts of ATH well dispersed and distributed particles (less than 1 micron), contribute to a more efficient work as char layer formers. Cone calorimetric results showed that for all investigated materials there is an important reduction in HRR, using ATH, ATH/ZB, ATH/ZB/OBEN as flame retardant additives. However, this behavior is not accompanied by lower flammability as UL94-V results showed.

3.6. Rheological properties

Rheological behavior in shear and oscillatory flow was studied in PE, PE-ATH$_{50}$, PE-ATH$_{30}$/ZB$_3$, PE-ATH$_{30}$/ZB$_3$/US, PE-ATH$_{30}$/ZB$_3$/OBEN$_2$ and in PE-ATH$_{30}$/ZB$_3$/OBEN$_2$/US materials. Fig. 7 shows shear viscosity as a function of shear rate. PE and PE-ATH$_{50}$ materials, present a nearly Newtonian-like behavior (constant viscosity) at low shear rate and a shear thinning behavior at high shear rate. Materials with lower ATH content (30 phr) obtained by TS showed an increase in the shear viscosity in the low shear rate range with respect to PE and PE-ATH$_{50}$. However at high shear rate they presented similar shear thinning behavior. Materials obtained by SS-TS presented two shear thinning zones: the first one at low shear rate (0.10-1.0 1/s), where the viscosity is higher than PE and materials obtained by TS. A high viscosity at low shear rate is attributed to a 3D entanglement structure where polymer chain mobility is restricted by effect of well dispersed and distributed particles with more surface area exposed by the ultrasound effect, therefore the particle–matrix interactions are increased. This structure is easily disrupted by flow. The second shear thinning zone is presented at high shear rate (1.0-100 1/s), with similar behavior of PE and

Table 6
Cone calorimetric results of selected materials.

Sample	TTI [s]	pkHRR [kW/m^2]	THE [MJ/m^2]	TSR [m^2/m^2]	CO yield [kg/kg]	CO$_2$ yield [kg/kg]	Residue [%]
Average st. dev.	±5	±18	±1.3	±44	±0.0006	±0.03	±0
PE	85	896	133	863	0.0269	3.22	0
PE-ATH$_{50}$	65	477	119	945	0.0293	3.90	20
PE-ATH$_{30}$/ZB$_3$	61	581	121	1052	0.0292	3.59	15
PE-ATH$_{30}$/ZB$_3$/US	72	545	123	981	0.0271	3.62	15
PE-ATH$_{30}$/ZB$_3$/OBEN$_2$	65	526	119	960	0.0283	3.75	18
PE-ATH$_{30}$/ZB$_3$/OBEN$_2$/US	69	503	119	1053	0.0270	3.71	18

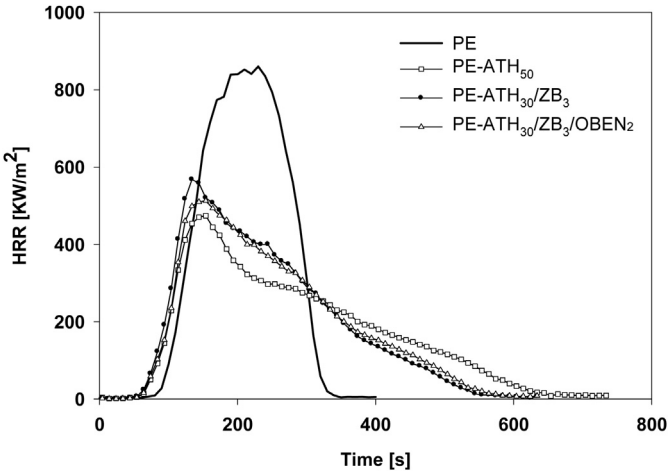

Fig. 5. Heat release rate as a function of time for PE, PE-AH$_{50}$, PE-AH$_{30}$/ZB$_3$ and PE-ATH$_{30}$/ZB$_3$/OBEN$_2$ materials (TS process).

materials extruded by TS, where shear forces are causing disentanglement of polymer chains and flow orientation and thus reducing the viscosity levels.

Fig. 8 shows the complex viscosity as a function of angular frequency under oscillatory flow measurements (SAOS flow). According to Fig. 8, the materials obtained by SS-US (PE-ATH$_{30}$/ZB$_3$/US and PE-ATH$_{30}$/ZB$_3$/OBEN$_2$/US) presented higher complex viscosity than materials obtained by TS. The PE-ATH$_{30}$/ZB$_3$/US material showed the highest complex viscosity in the whole shear rate range; meanwhile, the PE-ATH$_{30}$/ZB$_3$/OBEN$_2$/US material showed high complex viscosity in the low shear rate region. The materials obtained by TS showed similar complex viscosity pattern (curve overlapping). Swain and Isayev [8] attributed the increase of the complex viscosity of sonicated nanocomposites materials in the low frequency region (0.1–1.0 rad/s) to the improved interaction of the particles with the HDPE matrix due to the improved compatibilization effect brought about by ultrasound in HDPE/clay system, where the mobility of polymer chains is reduced due to particles dispersed at the nanometric level. For the PE-ATH$_{30}$/ZB$_3$/US and PE-ATH$_{30}$/ZB$_3$/OBEN$_2$/US materials, the increase in complex viscosity is attributed to improved interactions of the additive and OBEN particles with the PE matrix, probably at low frequency, the system present emulsion-like behavior due to reduction of particle size and improved dispersion and distribution. These results are in

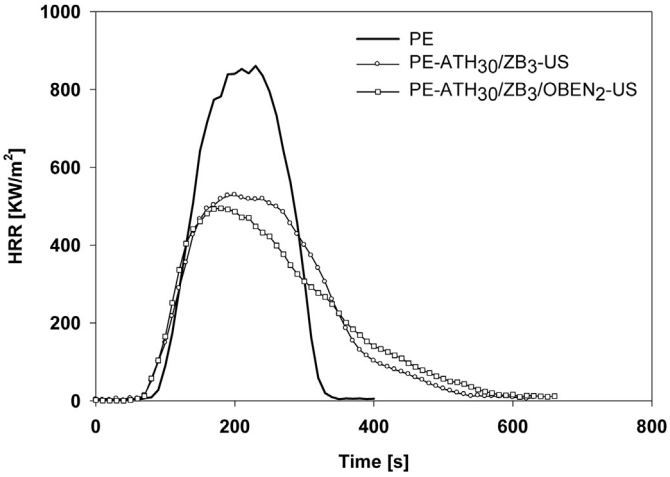

Fig. 6. Heat release rate as a function of time for PE, PE-AH$_{30}$/ZB$_3$/US and PE-AH$_{30}$/ZB$_3$/OBEN$_2$ materials (SS-US process).

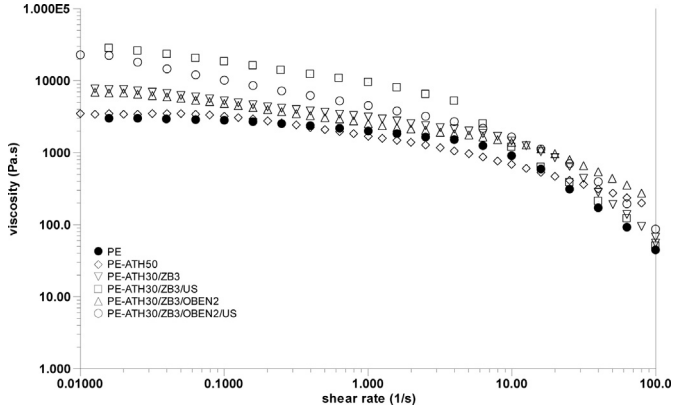

Fig. 7. Simple shear viscosity as a function of shear rate for the investigated materials.

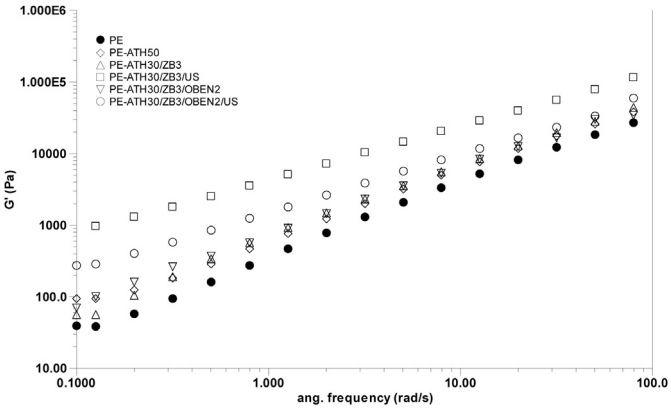

Fig. 9. Storage modulus (G′) as a function of frequency in SAOS flow.

agreement with the previous morphological study, where materials obtained by SS-US showed improved particle dispersion and distribution, as well as good affinity with the polymer matrix.

Fig. 9 presents the storage modulus (G′) as a function of angular frequency. According to Fig. 9, The three materials obtained by TS showed a slight increase of G′ with respect to PE, revealing that the type of additive and the additive content do not influence the elastic behavior; however when the materials are obtained by SS-US, a more elastic structure is produced since G′ is clearly higher for these materials than for TS materials in the 0.1–10.0 rad/s frequency range. As before, this effect is attributed to an increase in the particle–matrix interaction due to the better dispersion and distribution of the particles (ATH, ZB and OBEN) in the polymer matrix [6]. This result is also consistent with previous works [20] that reported an increase in G′ for well dispersed intercalated and exfoliated nanocomposites.

Fig. 10 depicts the Cole–Cole diagram, where the curves for materials obtained by SS-US deviate from the semicircle. This behavior has been previously reported to be associated with strong particle–matrix interaction in polymer composites [21] and also it has been associated to finer droplet-matrix morphology in polymer–elastomer blends [22]. This result confirms the enhanced dispersed and finer particle morphology obtained by ultrasound application.

3.7. Mechanical properties

Table 7 discloses mechanical properties of PE, PE-ATH_{50}, PE-ATH_{30}/ZB_3, PE-ATH_{30}/ZB_3/US, PE-$ATH_{30}/ZB_3/OBEN_2$ and PE-$ATH_{30}/ZB_3/OBEN_2$/US materials. As it has been mentioned before, one of the main problems in highly loaded flame retardant polymers is the negative effect on mechanical properties as it is clearly observed in Table 6, where PE-ATH_{50} material (with the highest ATH content) presents poor mechanical properties. Although the Young's modulus is high, indicating a more rigid highly-loaded material, the rest of the properties (Izod impact resistance, tensile strength, strain at break and tenacity) have the lowest values. When the ATH concentration is reduced to 30 phr, Young's modulus is diminished around 50%, as it was expected, with respect to PE-ATH_{50}. the PE-ATH_{30}/ZB_3 material presented increasing impact resistance after ultrasound application (from 52 to 63 J/m) derived from better dispersion and distribution of ATH particles. The PE-$ATH_{30}/ZB_3/OBEN_2$/US material attained the best mechanical performance with respect to a traditional flame retardant polymer using high ATH content (PE-ATH_{50}). Izod impact resistance increased from 53 to 85 J/m, tensile strength from 22 to 29 MPa, strain at break from 43 to 210% and tenacity from 7 to 38 MPa. These results showed that the use of the on-line ultrasound on the materials has an important effect on the mechanical properties and this effect is attributed to a good dispersion and distribution of flame retardant additives and OBEN. According to the enhanced mechanical properties, clay particles were dispersed probably up to the nanometric scale. Better compatibility between ATH-matrix-OBEN, as it was shown by morphological analysis, was another important feature to achieve this improvement in mechanical properties.

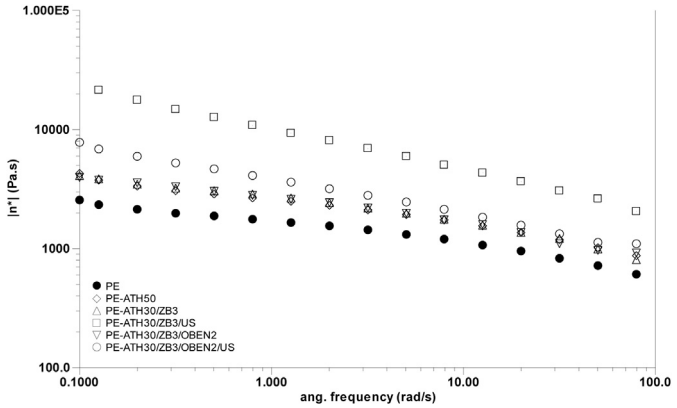

Fig. 8. Complex viscosity as a function of angular frequency in SAOS flow.

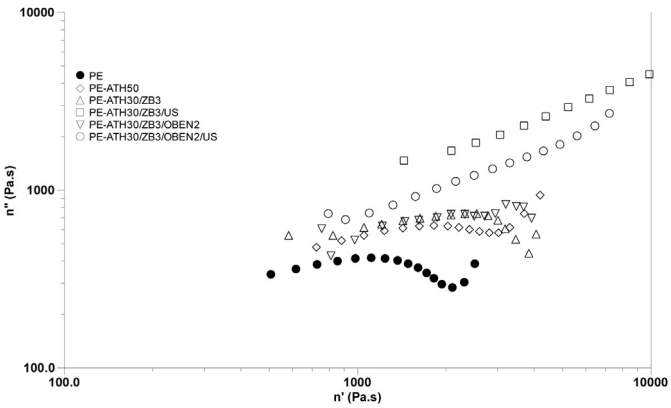

Fig. 10. Cole–Cole diagram (η″ vs η′) for investigated materials.

Table 7
Mechanical properties of investigated materials.

Sample	Izod impact resistance [J/m]	Young's modulus [MPa]	Tensile strength [MPa]	Strain at break [%]	Tenacity [MPa]
PE	153	1054	25	>500	>78
PE-ATH_{50}	53	1772	22	43	7
PE-ATH_{30}/ZB_3	52	814	23	200	32
PE-ATH_{30}/ZB_3/US	63	877	27	191	31
PE-$ATH_{30}/ZB_3/OBEN_2$	49	867	28	52	10
PE-$ATH_{30}/ZB_3/OBEN_2$/US	85	934	29	210	38

4. Conclusion

In this work, the effect of the on-line ultrasound application during the extrusion process of HDPE with flame-retardant additives (ATH, ZB and OBEN) was studied in detail. The investigation demonstrated that the on-line ultrasound application using a special mixer die modified the morphology of the compounding materials, due to a considerable reduction in the size of ATH particles (smaller than 1 micron) and improved particle dispersion and distribution. This effect has a remarkable influence on flame retardant properties, according to UL94 test in horizontal and vertical positions, because most of the materials obtained changed from HB to UL94-V2, and a V0 rating was achieved with the addition of 2 phr OBEN (PE-$ATH_{30}/ZB_3/OBEN_2$/US). Thermal analysis, oxygen index and cone calorimetric tests, showed similar behavior to that of traditional high loaded flame retardant materials (PE-ATH_{50}). The improved particle dispersion and finer particle morphology were confirmed by simple shear and small-amplitude oscillatory flow, assessing the presence of elastic materials with strong particle–matrix interactions. The use of a static mixer die ultrasonic device during single screw extrusion process, not only changed the morphology and improved flame retardant properties of the materials, but also increased the Izod impact resistance, tensile strength, strain at break and tenacity. Therefore, it was found that ATH content in PE matrix can be reduced from 50 phr (typical high concentration) to 30 phr (21.5 wt%), rendering an optimized flame retardant materials based on high density polyethylene.

Acknowledgments

We thank the financial support from the GTO-2011-C04-167285 Project and also we acknowledge the technical support of Dr. Omar Novelo Peralta for SEM analysis.

References

[1] Wilkie CA, Morgan AB, editors. Fire retardancy of polymeric materials. Boca Raton: CRC Press; 2010. p. 163–7.
[2] Kiliaris P, Papaspyrides CD. Polymer/layered silicate (clay) nanocomposites: an overview of flame retardancy. Prog Polym Sci 2010;35:902–58.
[3] Shen KK, Kochesfahani S, Jouffret F. Zinc borate as multifunctional polymer additives. Polym Adv Technol 2008;19:469–74.
[4] Bourbigot S, Le Bras M, Leeuwendal R, Shen KK, Schubert D. Recent advances in the use of zinc borate in flame retardancy of EVA. Polym Degrad Stab 1999;64:419–25.
[5] Hull TR, Quinn RE, Areri IG, Purser DA. Combustion toxicity of fire retarded EVA. Polym Degrad Stab 2002;77:235–42.
[6] Isayev AI, Kumar RK, Lewis TM. Ultrasound assisted twin screw extrusion of polymer-nanocomposites containing carbon nanotubes. Polymer 2009;50:250–60.
[7] Peng B, Wu H, Bao W, Gou S, Chen Y, Huang H, et al. Effects of ultrasound on the morphology and properties of propylene-based plastomer/nanosilica composites. Polym J 2011;43:91–6.
[8] Swain SK, Isayev AI. Effect of ultrasound on HDPE/clay nanocomposites: rheology, structure and properties. Polymer 2007;48:281–9.
[9] Sanchez-Olivares G, Sanchez-Solis A, Calderas F, Medina-Torres L, Herrera Valencia EE, Rivera-Gonzaga A, et al. Extrusion with ultrasound applied on intumescent flame-retardant polypropylene. Polym Eng Sci 2013 [published online].
[10] Cuadros J, Aldega L, Vetterlein J, Drickamer K, Dubbin W. Reactions of lysine with montmorillonite at 80 °C: implications for optical activity, H + transfer and lysine-montmorillonite binding. J Colloid Interface Sci 2009;333:78–84.
[11] Kitadai N, Yokoyama T, Nakashima S. In situ ATR-IR investigation of L-lysine adsorption on montmorillonite. J Colloid Interf Sci 2009;338:395–401.
[12] Parbhakar A, Cuadros J, Sephton MA, Dubbin W, Coles BJ, Weiss D. Adsorption of L-lysine on montmorillonite. Colloid Surf A 2007;307:142–9.
[13] Shi D, Yang J, Yao Z, Wang Y, Huang H, Jing W, et al. Functionalization of isotactic polypropylene with maleic anhydride by reactive extrusion: mechanism of melt grafting. Polymer 2001;42:5549–57.
[14] Ristolainen N, Hippi U, Seppälä J. Polym Eng Sci 2005;45:1568–75.
[15] Ramazani Ahmad SA, Rahimi A, Frounchi M, Radman S. Investigation of flame retardancy and physical-mechanical properties of zinc borate and aluminum hydroxide propylene composites. Mater Des 2008;29:1051–6.
[16] Formicola C, De Fenzo A, Zarrelli M, Frache A, Giordano M, Camino G. Synergistic effects of zinc borate and aluminium trihydroxide on flammability behavior of aerospace epoxy system. Express Polym Lett 2009;3(6):376–84.
[17] Schartel B, Bartholomain M, Knoll U. Some comments on the main fire retardancy mechanisms in polymer nanocomposites. Polym Adv Technol 2006;17:772–7.
[18] Schartel B, Braun U. Comprehensive fire behavior assessment of polymeric materials based on cone calorimeter investigations. e-Polymers 2003;13:1–14.
[19] Shartel B, Hull R. Development of fire-retarded materials-Interpretation of cone calorimetric data. Fire Mater 2007;31(5):327–54.
[20] Riva A, Zanetti M, Braglia M, Camino G, Falqui L. Thermal degradation and rheological behaviour of EVA/montmorillonite nanocomposites. Polym Degrad Stab 2002;77:299–304.
[21] Zhou Z, Zhang Y, Zhang Y, Yin N. Rheological behavior of polypropylene/octavinyl polyhedral oligomeric silsesquioxane composites. J Polym Sci Part B 2008;46:526–33.
[22] Peyman E, Ismaeil G, Mohammad K, Hamed A. Rheological behaviour of PP/EPDM blend: the effect of compatibilization. Iran Polym J 2008;17(9):669–79.